INSTITUTE OF PHYSICS PUBLISHING PLASMA PHYSICS AND CONTROLLED FUSION

Plasma Phys. Control. Fusion **43** (2001) A277–A286 PII: S0741-3335(01)29911-4

Inferences of mix in direct-drive spherical implosions with high uniformity

D D Meyerhofer[1,5], J A Delettrez[1], R Epstein[1], V Yu Glebov[1], V N Goncharov[1], R L Keck[1], R L McCrory[1], P W McKenty[1], F J Marshall[1], P B Radha[1], S P Regan[1], S Roberts[1], W Seka[1], S Skupsky[1], V A Smalyuk[1], C Sorce[1], C Stoeckl[1], J M Soures[1], R P J Town[1], B Yaakobi[1], J A Frenje[2], C K Li[2], R D Petrasso[2,6], F H Séguin[2], K Fletcher[3], S Padalino[3], C Freeman[3], N Izumi[4], R A Lerche[4], T W Phillips[4] and T C Sangster[1,4]

[1] Laboratory for Laser Energetics, University of Rochester, 250 East River Road, Rochester, NY 14623-1299, USA
[2] Plasma Science and Fusion Center, MIT, Cambridge, MA 02139, USA
[3] State University of New York at Geneseo, Geneseo, NY 14454, USA
[4] Lawrence Livermore National Laboratory, 7000 East Avenue, Livermore, CA 94550, USA

Received 22 June 2001
Published 22 November 2001
Online at stacks.iop.org/PPCF/43/A277

Abstract

A large number of diagnostics have been used to study the performance of gas-filled, plastic-shell direct-drive implosions on the 60-beam OMEGA laser system (Boehly T R *et al* 1997 *Opt. Commun.* **133** 495). These diagnostics allow an estimate of the amount of fuel–pusher mixing in the compressed core. Implosions have primary neutron yields and fuel areal densities that are ∼35% and ∼100% of the predicted one-dimensional values, respectively. A highly constrained model of the core conditions and fuel–shell mix has been developed. It suggests that there is a 'clean' fuel region surrounded by a mixed region, with the clean region accounting for ∼70% of the fuel areal density.

1. Introduction

In the direct-drive approach to laser-driven inertial confinement fusion (ICF) [1], a spherical target is symmetrically illuminated by a number of individual laser beams. Target surface and laser illumination uniformity are the primary determinants of target performance. Illumination uniformity includes both individual-beam uniformity and on-target, beam-to-beam power history differences (power balance), while target non-uniformities include those on both the inner and outer capsule surfaces. Non-uniformities lead to distortions in the compressed core due to secular growth of low-order ($l \leqslant 10$) modes and shell breakup and mix due to

[5] Also Departments of Mechanical Engineering and Physics and Astronomy, University of Rochester
[6] Also Visiting Senior Scientist, Laboratory for Laser Energetics, University of Rochester

 © 2001 IOP Publishing Ltd Printed in the UK

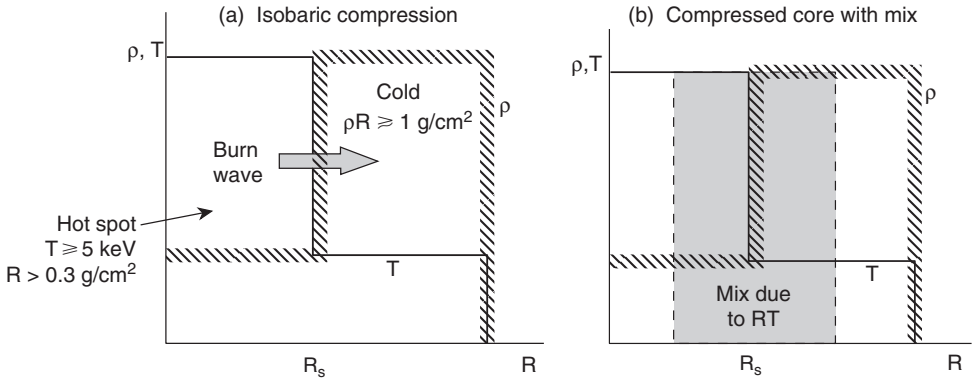

Figure 1. (*a*) Idealized temperature and density profiles in the compressed core of an ICF implosion relying on isobaric compression and 'spark' ignition. (*b*) Idealized core temperature and density profiles for isobaric compression in the presence of the RT instability and mix.

the Rayleigh–Taylor (RT) [2, 3] growth of perturbations imprinted by high-order ($l > 10$) non-uniformities. Direct-drive ICF targets are unstable to the RT instability during both the acceleration and deceleration phases of the implosion [4]. Ignition with direct-drive (and indirect drive) ICF relies on the generation of a 'spark' in the compression 'hot spot' to begin the nuclear burn process [4]. The hot spot is a high-temperature, low-density region surrounded by a low-temperature, high-density region into which the burn wave propagates, leading to significant energy gain. Figure 1(*a*) shows the idealized profiles of the isobaric compressed core. The non-linear evolution of the RT instability determines the characteristics of the compressed core. In particular, it can lead to significant distortions in the fuel–pusher boundary and mix of the fuel and pusher material (see figure 1(*b*)). For an ICF target to ignite, a significant fraction of the hot spot must remain 'clean', unperturbed by the evolution of the RT instability.

This paper presents results of a series of direct-drive implosions of gas-filled plastic shells on the OMEGA laser system [5] designed to study the effect of the RT instability on compressed cores. These targets are surrogates [6, 7] for cryogenic implosions that have recently commenced on OMEGA. The goal of these experiments is to vary the target constituents without varying the hydrodynamic performance to allow a large number of diagnostics to be utilized to infer the amount of fuel–pusher mixing in the compressed core. It is found that for the implosion results presented here, approximately 70% of the hot spot remains clean, unaffected by mixing.

Section 2 describes the targets, diagnostics, and laser conditions applied to the spherical implosions. Section 3 describes the target performance, and section 4 presents a static mix model. The paper is summarized in section 5.

2. Targets, diagnostics, and laser conditions

The philosophy of the experiments reported here is to first choose a laser pulse shape, smoothing conditions, target-shell thickness, and gas-fill pressure to provide hydrodynamic conditions close to those of cryogenic targets. The makeup of the fill gas or details of the shell layers are varied so that many diagnostics can be applied to the nearly identical implosions. OMEGA produces very reproducible implosions, suggesting that the implosion hydrodynamics is similar for different target types and fill-gas makeup. In the results presented here, the targets were $\sim$940 μm diameter shells of 20 μm thick plastic, primarily CH, with some shells having

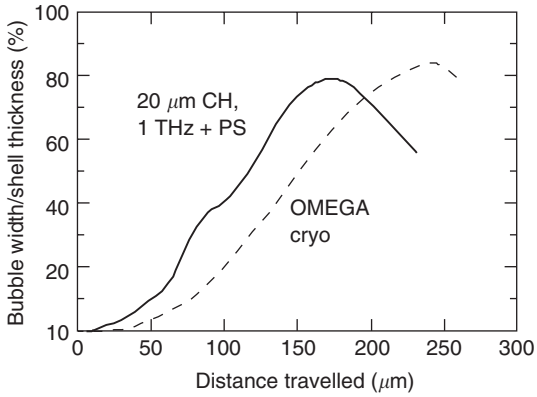

Figure 2. Ratio of the calculated acceleration phase 'mix' width to the in-flight shell thickness for 20 CH shells illuminated by 1 ns square pulses with 1 THz SSD and PS (——). A similar comparison for NIF-scaled cryogenic targets planned for OMEGA (- - - -).

embedded CD layers. The targets were filled with 15 atm of various hydrogenic species (D_2, DT, etc.), some doped with trace amounts of Ar, or with He^3 or D-He^3. In the latter case, the pressure was adjusted so that the characteristics of the deceleration phase, which is determined by the electron and ion pressure, were the same.

An important measure of target stability during the acceleration phase is the ratio of the amplitude of the ablation-surface mix width to the in-flight shell thickness. The smaller this ratio, the more stable the implosion. Figure 2 shows this ratio calculated for the plastic-shell-implosion conditions used in this experiment (solid line) and for a cryogenic-target implosion planned for OMEGA (dashed line). The in-flight shell thickness was calculated using the one-dimensional hydrodynamic code *LILAC* [8], and the mix width was calculated using a post-processor that includes the effects of mass ablation, finite shell thickness, and spherical convergence [9]. In implosions of 20 μm thick, gas-filled plastic shells driven with a 1 ns square laser pulse, the ratios of the thickness of the ablation-surface mix region due to RT growth to the in-flight shell thickness are similar to those predicted for OMEGA cryogenic implosions. Plastic shells allow a wide variety of shell/gas conditions and diagnostics can be applied to study the details of the implosion [10–12]. This is not possible with cryogenic targets.

2.1. Core diagnostics

The primary (N_p) and secondary neutron (N_s) yields were measured using scintillator counters coupled to fast photomultipliers [13]. Indium and copper activation provided additional yield measurements [14]. For the range of yields recorded, the typical uncertainty in these measurements was 10%. The fast scintillator counters also measured the neutron-averaged ion temperature with an uncertainty of $\sim$0.5 keV.

The secondary proton and knock-on particle yields were measured with filtered range filters [15] and charged-particle spectrometers (CPS) [16]. CR-39 nuclear emulsion was used in both detectors to determine the yield and the energy spectrum.

For DT-filled implosions, the fuel areal density is determined from the number of elastically scattered knock-on fuel particles [17, 18]:

$$\mathrm{n} + \mathrm{T(D)} \rightarrow \mathrm{n}' + \mathrm{T}'(\mathrm{D}'). \tag{1}$$

The yield of knock-on particles is insensitive to the electron temperature profile [17, 18].

Limits on fuel areal density (ρR_f) in D_2-filled implosions can be inferred from the two-step secondary neutron (N_s) production [15, 19]

$$D + D \rightarrow T + p \tag{2}$$

followed by

$$T + D \rightarrow n(12\text{–}17\,\text{MeV}) + {}^4\text{He}, \tag{3}$$

and two-step secondary proton production (p_s) [15, 19]

$$D + D \rightarrow {}^3\text{He} + n \tag{4}$$

followed by

$${}^3\text{He} + D \rightarrow p(12\text{–}17\,\text{MeV}) + {}^4\text{He}. \tag{5}$$

The secondary proton and neutron yields depend on the electron temperature profile in the core and typically provide limits on the ρR_f and the core electron temperature, as well as provide information about the temperature and density profiles [15, 19].

The inferred value of ρR_f depends on whether a hot-spot (point-like source surrounded by uniform fuel) or uniform (uniform fuel and source) 'ice-block' model is used. The ρR_f inferred with the uniform model is ∼34% larger than with the hot-spot model [15, 19]. Simulations using *LILAC* [8] suggest that the uniform model is more appropriate for inferring ρR_f under the experimental conditions described in this work.

2.2. Shell diagnostics

The areal density of the plastic shell, ρR_s, during stagnation was measured with charged particle spectroscopy. Secondary protons from D_2 implosions (produced with 12–17 MeV energies) are slowed down predominantly in the shell by an amount proportional to ρR_s [15]. For CH shells with DT fill, the number of knock-on protons determines ρR_s [18]. In addition, knock-on deuterons and tritons are slowed in the shell, providing another measure of ρR_s and, coupled with the knock-on proton yield, an estimate of the shell electron temperature [18].

2.3. Mix diagnostics

The core–fuel mix characteristics are inferred in a number of ways. CD layers in D_2-filled CH targets are probed with tritons and ^{3}He particles produced in the D_2 reaction in the fuel region (equations (2)–(5)) [20]. The measured secondary yields from the shell regions are compared to one-dimensional simulations. When the yields are significantly different than those predicted, they provide information about fuel–shell mix. The secondary DT neutrons and D-^{3}He protons produced directly in the shell can be subtracted using H_2-filled implosions with the same shell conditions. An implosion of a plastic shell with a CD layer and a pure-^{3}He fill provides a primary D-^{3}He proton signal only if the shell and fuel regions are microscopically mixed. This yield depends on the characteristics of the mix, either microscopic (diffusive) or macroscopic, where islands of shell material penetrate the core.

2.4. Spectroscopic diagnostics

In some cases, the 15 atm D_2 fuel was doped with 0.05 atm Ar. This level of Ar dopant has a negligible effect on target performance. Time-resolved Ar K-shell spectra were diagnosed

with a flat crystal spectrometer coupled to an x-ray streak camera with 25 ps resolution. The emissivity-averaged core electron temperature and density evolutions were inferred from the time-dependent Ar K-shell spectral line shapes of the Ar He-β ($1s3l$–$1s^2$), He-γ ($1s4l$–$1s^2$), He-δ ($1s5l$–$1s^2$), and Ly-β ($3l$–1s) resonant transitions and associated satellites [21]. The line shapes depend strongly on the electron density and are relatively insensitive to the electron temperature, while the relative line intensities are sensitive to variations in both electron temperature and density [22]. The electron temperature and densities were obtained by fitting the line shapes and intensities to a radiation model following [21, 23].

2.5. Laser conditions

An ~23 kJ, 1 ns square pulse delivered by the 60-beam OMEGA laser system [5] was used to drive the implosions described in this work. The beam-to-beam UV energy balance is typically $\leqslant$5% rms [24]. When beam overlap on target is included, the on-target non-uniformity due to beam-to-beam power imbalance is <2% (l-mode $\leqslant$ 12). Individual-beam smoothing was accomplished by combining distributed phase plates (DPP) [25], polarization smoothing (PS) with birefringent wedges [26], and smoothing by spectral dispersion (SSD) [27]. The DPPs produce a third-order super-Gaussian profile with 95% of the energy enclosed in an ~936 μm diameter spot. When two-dimensional SSD and PS are added, the spot diameter increases somewhat because of the angular divergence associated with these techniques. The two-dimensional SSD had a single colour cycle with 1 THz bandwidth at 3 GHz and 10 GHz modulation frequencies.

The calculated time-dependent, on-target non-uniformity (l = 1–500) due to single-beam non-uniformity assuming perfect beam-to-beam power balance for 1 THz SSD with PS is less than 1% after 300 ps [28]. Additional on-target non-uniformities are caused by beam-to-beam power imbalance and differences in DPP spot sizes.

3. Implosion results

The results of a series of implosions of the shells described above are presented in this section. Different information is obtained from different target compositions. In all cases, however, the fill pressure and overall shell thickness are the same. These implosions have a calculated convergence ratio (initial to final radius of the fuel–shell boundary) of 15. Further information about these implosions, including comparisons of target performance for different smoothing conditions, can be found in [24]. The ratios of the measured primary neutron yield to that predicted by one-dimensional simulations ('yield over clean' (YOC)) for CH shells with D_2 fills show good reproducibility and are about 35% [24]. The implosions with 15 atm filled, 20 μm thick shells were taken over three experimental campaigns spanning two months and show an ~10% standard deviation of the YOCs.

For 20 μm thick CH shells with 15 atm D_2 or DT fill pressures, the predicted ρR_f is 16 mg cm^{-2} and ρR_s is 60 mg cm^{-2}. The measured charged-particle spectra used to determine the fuel, shell, and total areal densities of these implosions are shown in figure 3. Figures 3(a) and (b) show the measured knock-on D and p spectra for CH shells filled with DT. The ρR_f inferred from D knock-on yield is 16 mg cm^{-2}, while $\rho R_s \sim 61$ mg cm^{-2} from the knock-on protons. The total ρR, which is determined from the slowing down of D-^{3}He secondary protons from D_2-filled shells (figure 3(c), is 76 mg cm^{-2}. These measurements show that the sum of fuel and shell areal densities for DT implosions is in good agreement with the total areal density independently inferred from D_2 implosions. The measured fuel and shell areal densities are close to those predicted from one-dimensional simulations.

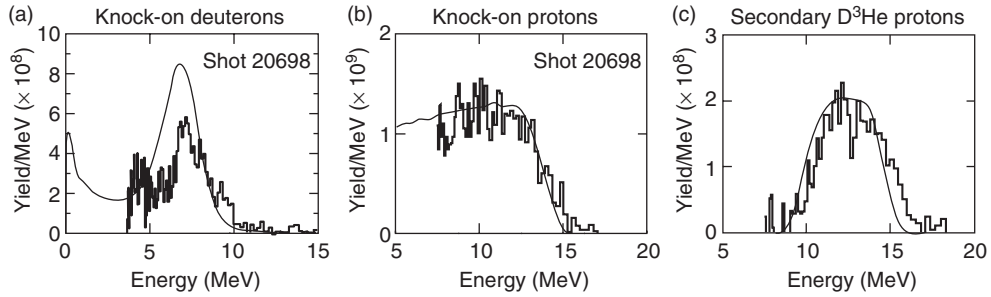

Figure 3. Various measurements of shell and fuel areal density, with the one-dimensional simulation predictions shown as thin solid lines: (*a*) The measured 'knock-on' deuteron spectrum for a 15 atm DT fill in a 20 μm thick CH shell. The estimated fuel areal density is 16 mg cm^{-2} [18]. (*b*) The measured knock-on proton spectrum for a 15 atm DT fill in a 20 μm thick CH shell. The estimated shell areal density is 61 mg cm^{-2} [18]. (*c*) The measured secondary D-^{3}He proton spectrum for a 15 atm D_2 fill in a 20 μm thick CH shell. The estimated total areal density is 76 mg cm^{-2} [15].

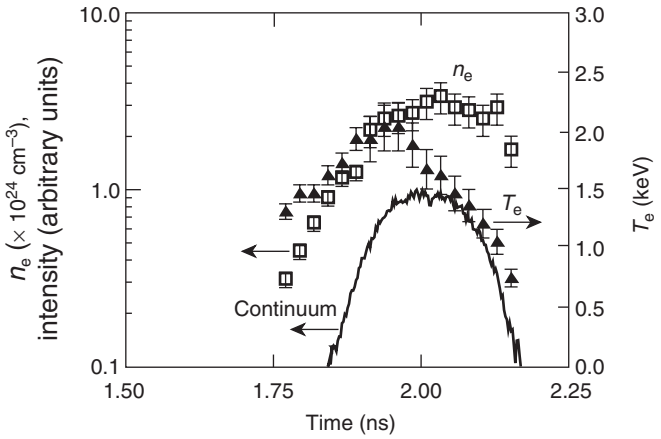

Figure 4. Temporal evolution of the emissivity-averaged core electron temperature and density near peak compression. The temporal evolution of the ∼3.5 keV continuum emission is also shown.

As described in section 2.4, the emissivity-averaged electron temperature and density history were inferred from spectroscopic measurements of Ar-doped capsules. Figure 4 shows the evolution of the emissivity-averaged electron temperature and density during peak compression. The evolution of the continuum emission at ∼3.5 keV is also shown [21]. Note that peak neutron emission occurs ∼170 ps before the peak continuum emission (consistent with one-dimensional simulations).

The amount of fuel–pusher mixing can be inferred by combining the measurements of the fuel areal density (figure 3(*a*)), the core size from x-ray emission (∼34 μm), and the electron density from spectroscopic analysis (figure 4) [21]. This analysis gives an average D_2 density of 4.4 ± 1.3 g cm^{-3} and a CH density of 2.6 ± 0.8 g cm^{-3} in the emission region, suggesting that the compressed core is approximately one-third mixed. This analysis, however, provides no information about the spatial profiles in the core. Mix profiles in the core are inferred in the next section.

4. Core-mix model

The preceding sections have presented various experimental results for the performance of 20 μm thick, ~940 μm diameter CH shells with 15 atm of gas fill. These have been combined to estimate that the compressed fuel region is two-thirds and D_2 one-third CH. While some observations are close to those predicted by one-dimensional hydrodynamic simulations, others, such as the primary yield, are lower, while still others, such as the ratio of the secondary neutron yield to the primary neutron yield, are larger. The variation in observables provides constraints on the possible core conditions and fuel–pusher mix during stagnation. In this section, the experimental results are compared to a one-dimensional static model of the core to gain additional insight about target performance (a refined version of the model described in [24, 29]).

The model assumes that the compressed core at the time of peak neutron production can be divided into two regions: a 'clean' region with only fuel material and a 'mixed region' where some of the shell material is mixed with the fuel material (see figure 5). The clean region is characterized by a fuel density and radius. In the mix region, the fuel density decreases linearly from the edge of the clean region to the edge of the mix region and the shell material density decreases linearly from the edge of the mix region to the edge of the clean region. The temperature profile is assumed to be of Gaussian shape, and the electron and ion temperatures are assumed to be the same. Thus, the model has six parameters: the density and radius of the clean region, the outer radius of the mix region, the shell density, the temperature in the centre, and the width of the Gaussian temperature profile. The total fuel mass is assumed to be conserved. The model calculates the relevant nuclear reactions and reaction product transport in the assumed density and temperature profiles.

The predictions of this model are compared with neutron-averaged observations. The nuclear and particle emission from the compressed core in the model must match the measured values of the primary neutron burn rate, the neutron-averaged ion temperatures, and the secondary neutron, proton, and knock-on yields. CH shells with inner CD layers filled with ^{3}He fuel provide additional experimental observations. Eight independent experimental observables are used to constrain the model's parameters.

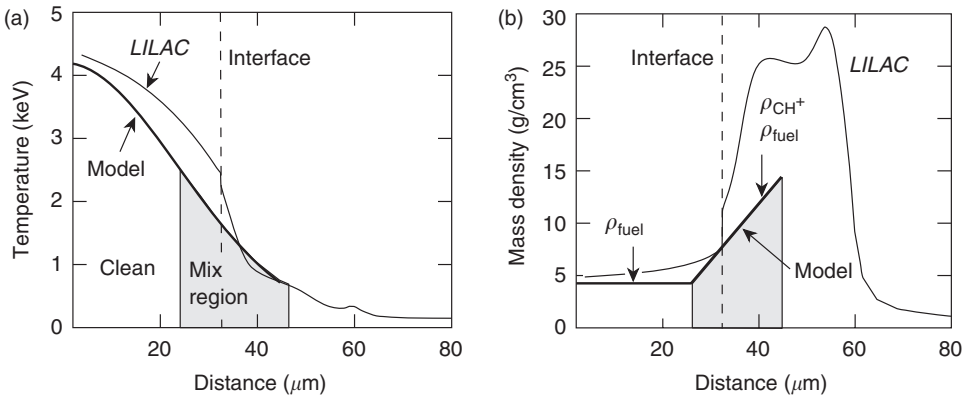

Figure 5. Inferred core and fuel–shell mix profiles from the mix model described in the text. The temperature profiles are shown in (*a*) and the density profiles in (*b*). The range of the parameters, which are consistent with the experimental observations, is shown by the width of the various parameter bands. The solid lines represent the predictions of one-dimensional hydrodynamic simulations at peak neutron production, assuming no mixing, and the vertical dashed lines show the location of the fuel–shell interface in the one-dimensional simulations.

Table 1. Comparison of measured and mix-model-predicted implosion parameters for ∼19 μm thick CH shells (with and without CD layers) filled with 15 atm of D_2, DT, or ^{3}He for implosions with 1 THz SSD and polarization smoothing

Parameter	Measurement	Model (% of expt)
Fuel ρR (mg cm^{-2})	15 ± 3	100
Maximum neutron burn rate (n s^{-1})	$(9 \pm 2) \times 10^{20}$	120
T_{ion} (D_2) (keV)	3.7 ± 0.5	90
Secondary neutron ratio	$(2.1 \pm 0.4) \times 10^{-3}$	90
Secondary proton ratio	$(1.8 \pm 0.3) \times 10^{-3}$	100
D-^{3}He proton yield (^{3}He fill)	$(1.0 \pm 0.2) \times 10^7$	100
D_2 neutron yield (^{3}He fill)	$(4.5 \pm 1.5) \times 10^8$	135
T_{ion} (CD) (keV)	1.7 ± 0.5	110

The core temperature and density profiles shown as heavy lines in figure 5 correspond to inferences from this model for 15 atm filled, 20 μm thick, plastic shells. This figure also shows one-dimensional *LILAC* predictions at the time of peak neutron production for the electron temperature and density profiles and (vertical dashed lines) the location of the fuel–pusher interface. The measured values of the eight parameters and their fraction (in per cent) predicted by the model are shown in table 1. The model predicts that the total compressed radius is 45 μm with approximately 1 μm (20% of the compressed shell areal density) of the original shell material mixed into the outer 30% of the *LILAC*-calculated fuel region. The remainder of the fuel region is 'clean'.

The centre of the calculated mix region shown in figure 5 lies roughly at the position of the *LILAC*-predicted fuel–pusher interface as might be intuitively expected. In addition, the density profiles calculated with the model are close to the *LILAC* calculations, which is consistent with the measured total areal density being very close to the one-dimensional predicted value. In the future this model will be applied to other implosion conditions to further understand the mix characteristics. Work is in progress to incorporate the constraints provided by the spectroscopic results (described above) into the mix model.

5. Conclusions

In summary, the performance of 20 μm thick CH shells (15 atm fuel fill) with full beam smoothing (1 THz SSD and PS) on OMEGA has produced moderate-convergence-ratio (CR∼15) implosions that perform close to one-dimensional predictions. The primary neutron yield is ∼35–45% of that predicted, while the fuel and shell areal densities are close to their predicted values. The stagnation conditions are reproduced by a tightly constrained static mix model that suggests that ∼70% of the hot spot remains clean during the implosion. This model's predictions are consistent with nuclear, charged particle, and spectroscopic diagnostics. The results of ^{3}He-filled shells with CD layers suggest that microscopic (atomic scale) mixing is occurring in these implosions. The inference of an 'unmixed' region comprising ∼70% of the one-dimensional predicted hot-spot radius provides optimism for the performance of direct-drive cryogenic targets on the NIF.

Acknowledgments

The authors are extremely grateful to the staff of the Laboratory for Laser Energetics for their dedicated efforts in developing and providing the high-performance OMEGA laser system,

including low power imbalance, high single-beam uniformity, and high-quality diagnostics, operations, and target fabrication. This work was supported by the US Department of Energy Office of Inertial Confinement Fusion under Cooperative Agreement No DE-FC03-92SF19460, the University of Rochester, and the New York State Energy Research and Development Authority. The support of DOE does not constitute an endorsement by DOE of the views expressed in this paper.

References

[1] Nuckolls J, Wood L, Thiessen A and Zimmerman G 1972 Laser compression of matter to super-high densities: thermonuclear (CTR) applications *Nature* **239** 139–42

[2] Kilkenny J D, Glendinning S G, Haan S W, Hammel B A, Lindl J D, Munro D, Remington B A, Weber S V, Knauer J P and Verdon C P 1994 A review of the ablative stabilization of the Rayleigh–Taylor instability in regimes relevant to inertial confinement fusion *Phys. Plasmas* **1** 1379–89

[3] Bodner S E *et al* 1998 Direct-drive laser fusion: status and prospects *Phys. Plasmas* **5** 1901–18

[4] Lindl J D 1998 *Inertial Confinement Fusion: The Quest for Ignition and Energy Gain Using Indirect Drive* (New York: Springer) pp 61–82

[5] Boehly T R *et al* 1997 Initial performance results of the OMEGA laser system *Opt. Commun.* **133** 495–506

[6] Marshall F J, Delettrez J A, Glebov V Yu, Town R P J, Yaakobi B, Kremens R L and Cable M 2000 Direct-drive, hollow-shell implosion studies on the 60-beam, UV OMEGA laser system *Phys. Plasmas* **7** 1006–13

[7] Delettrez J A, Glebov V Yu, Marshall F J, Stoeckl C, Yaakobi B and Meyerhofer D D 1999 Effect of beam smoothing and pulse shape on the implosion of DD-filled CH shell targets on OMEGA *Bull. Am. Phys. Soc.* **44** 192–3

[8] Richardson M C *et al* 1986 Ablatively-driven targets imploded with the 24 UV beam OMEGA system *Laser Interaction and Related Plasma Phenomena* vol 7 ed H Hora and G H Miley (New York: Plenum) pp 421–48

[9] Goncharov V N, McKenty P, Skupsky S, Betti R, McCrory R L and Cherfils-Clérouin C 2000 Modeling hydrodynamic instabilities in inertial confinement fusion targets *Phys. Plasmas* **7** 5118–39

[10] Cable M D *et al* 1994 Indirectly driven, high convergence inertial confinement fusion implosions *Phys. Rev. Lett.* **73** 2316–19

[11] Bradley D K *et al* 1998 Measurements of core and pusher conditions in surrogate capsule implosions on the OMEGA laser system *Phys. Plasmas* **5** 1870–79

[12] Marshall F J *et al* 2000 Direct-drive high-convergence-ratio implosion studies on the OMEGA laser system *Phys. Plasmas* **7** 2108–13

[13] Glebov V Yu, Meyerhofer D D, Stoeckl C and Zuegel J D 2001 Secondary-neutron-yield measurements by current-mode detectors *Rev. Sci. Instrum.* **72** 824–7

[14] Lane S M, Jones B A, Selchow N J, Bennett C K, Nilson D G, Glendinning S G, Lerche R A, Singh M S, Derzon M S and Nelson M B 1987 Neutron activation yield detectors *Laser Program Annual Report* 1996 Lawrence Livermore National Laboratory, Livermore, CA, UCRL-50021-86, 3-100–3-102

[15] Séguin F H *et al* Using secondary proton spectra to study imploded D_2-filled capsules at the OMEGA laser facility *Phys. Plasmas* submitted

[16] Hicks D G 1999 Charged particle spectroscopy: a new window on inertial confinement fusion *PhD Thesis* Massachusetts Institute of Technology

[17] Skupsky S and Kacenjar S 1981 Measuring fuel ρR for inertial fusion experiments using neutron elastic-scattering reactions *J. Appl. Phys.* **52** 2608–13

[18] Li C K *et al* Study of direct-drive, DT gas-filled-plastic capsule implosions using nuclear diagnostics at OMEGA 2001 *Phys. Plasmas* **8** 4902–13

[19] Azechi H, Cable M D and Stapf R O 1991 Review of secondary and tertiary reactions and neutron scattering as diagnostic techniques for inertial confinement fusion targets *Laser Part. Beams* **9** 119–34

[20] Glebov V Yu, Delettrez J A, Epstein R, McKenty P W, Marshall F J, Meyerhofer D D, Radha P B, Smalyuk V A and Stoeckl C 1999 Evidence for fuel–pusher mixing in OMEGA direct-drive implosions by neutron diagnostic *Bull. Am. Phys. Soc.* **44** 194

[21] Regan S P *et al* 2001 Shell mix in compressed core of spherical implosion *Phys. Rev. Lett.* submitted

[22] Haynes D A Jr, Hooper C F Jr, Mancini R C, Bradley D K, Delettrez J, Epstein R and Jaanimagi P A 1995 Spectroscopic analysis of AR-doped laser-driven implosions *Rev. Sci. Instrum.* **66** 755–7

[23] Haynes D A Jr, Garber D T, Hooper C F Jr, Mancini R C, Lee Y T, Bradley D K, Delettrez J, Epstein R and Jaanimagi P A 1996 Effects of ion dynamics and opacity on stark-broadened argon line profiles *Phys. Rev.* E **53** 1042–50

[24] Meyerhofer D D *et al* 2001 Core performance and mix in direct-drive spherical implosions with high uniformity *Phys. Plasmas* **8** 2251–6

[25] Kessler T J, Lin Y, Armstrong J J and Velazquez B 1993 Phase conversion of lasers with low-loss distributed phase plates *Laser Coherence Control: Technology and Applications* vol 1870, ed H T Powell and T J Kessler (Bellingham, WA: SPIE) pp 95–104

[26] Boehly T R, Smalyuk V A, Meyerhofer D D, Knauer J P, Bradley D K, Craxton R S, Guardalben M J, Skupsky S and Kessler T J 1999 Reduction of laser imprinting using polarization smoothing on a solid-state fusion laser *J. Appl. Phys.* **85** 3444–7

[27] Skupsky S, Short R W, Kessler T, Craxton R S, Letzring S and Soures J M 1989 Improved laser-beam uniformity using the angular dispersion of frequency-modulated light *J. Appl. Phys.* **66** 3456–62

[28] Skupsky S and Craxton R S 1999 Irradiation uniformity for high-compression laser-fusion experiments *Phys. Plasmas* **6** 2157–63

[29] Radha P B, Glebov V Yu, Marshall F J, Meyerhofer D D, Regan S P, Seka W, Skupsky S, Smalyuk V A, Soures J M, Stoeckl C, Yaakobi B and Petrasso R D 2000 A measurement-based picture of core conditions in OMEGA implosions *Bull. Am. Phys. Soc.* **45** 164